Applied Geochemistry 97 (2018) 226–237

Contents lists available at ScienceDirect

Applied Geochemistry

journal homepage: www.elsevier.com/locate/apgeochem

Geoelectrochemical anomaly prospecting for uranium deposits in southeastern China

Panfeng Liu[a,b], Xianrong Luo[a,b,*], Meilan Wen[a,b], Jiali Zhang[a], Chaojie Zheng[a,b], Wen Gao[a,b], Fei Ouyang[a,b]

[a] College of Earth Sciences, Guilin University of Technology, Guilin, 541006, China
[b] Research Institute of Prediction of Hidden Deposits, Guilin University of Technology, Guilin, 541006, China

ARTICLE INFO

Editorial handling by Dr Q Gong

Keywords:
Uranium deposit
Uranium nanoparticles
Geoelectrochemical probe
Ore prospection

ABSTRACT

Most volcanogenic uranium deposits are deeply buried and very hard to locate. A prospecting method using geoelectrochemical probes has been proven in practice to be an effective way of pinpointing the locations of these hidden deep uranium deposits. The efficacy of the method has been verified through analyses of two carefully selected known uranium deposits: the Xiangshan and Shenyuan uranium deposits in southeastern China. Analyses of geoelectrochemical probe samples presented in transections crossing the ore bodies revealed distinct anomalies of U and Mo distribution. The average anomaly contrast values (the ratio of element concentration in the geoelectrochemical probe between potential areas and background areas) ranging from 1.5 to 2.3 corresponded perfectly with the locations of the known ore bodies in the deposit. Anomalies of Th, Pb, Zn, and Ag were also detected, confirming the viability and effectiveness of using the geoelectrochemical probe method to locate buried deposits. The geoelectrochemical anomaly detection was corroborated by detection of U-bearing mineral nanoparticles scavenged in the probe foams. A flotation mechanism using geogenic gas was suggested as the major driving force for the enrichment of the nanoparticles in the soil surface. Geogenic gas generated from fault belts and ore body differentiation (oxidation-reduction and weathering) is an as-yet neglected but potentially important mechanism for the formation of the anomalies.

1. Introduction

Uranium deposits in volcanic rocks are one of the four major uranium deposit types in China and account for 20% of the country's total uranium reserves (Fang, 2009; Fang et al., 2012). They are mostly found in the volcanic belts of Mount Tianshan in Xinjiang Autonomous Region, in the Great Khingan in northeastern China, and in southeastern China. The volcanic deposits in southeastern China are mostly deep-seated in felsic (or slightly basic) paleo-continental crust (Zhong et al., 2015). With overlaying layers of considerable thicknesses (usually more than a hundred or even several hundreds of metres), these deposits are difficult to find, as they only send out very weak "direct signals" for prospectors using conventional geochemical methods of exploration.

The geoelectrochemical method, one of several deep penetration geochemical prospecting techniques, has improved since its first application in volcanogenic uranium deposits in the Shengyuan (Jin et al., 2007) and Xiangshan (Wen et al., 2011; Li et al., 2012; Ke et al., 2014) areas of Jiangxi Province. A feasibility test of this method in the Dongsheng area of the Erdos Basin had positive results in exploring sandstone uranium deposits (Yao et al., 2012; Man et al., 2015). During an attempt to prospect for concealed uranium deposits with geoelectrochemical extractions and soil ionic conductivity measurements in the Huxi volcanogenic uranium deposit area of Lean County in Jiangxi Province, anomalous areas of electrical conductivity peak values with some geoelectro-extraction anomalies were discovered for ore-forming elements including U, Th, and Mo, along with some other metallic elements (Hou et al., 2012). In addition to the deposits located in China, a good match between geoelectro-extraction measurements and soil survey data of elements U, Mo and V was observed in the Four Mile East and Goulds Dam sandstone uranium deposits, Australia. It was also worth mentioning that Australian researchers noticed that in areas with weak geochemical anomalies, geoelectro-extraction anomalies were hard to ignore (Hou et al., 2012).

The geoelectrochemical method originated in the former Soviet Union. The theory underlying this method was first proposed by Safronov N.I., who posited that an artificial electric field can be applied to the deep concealed ore bodies and draw metal ion migration to the

* Corresponding author. Guilin University of Technology, College of Earth Sciences, 319 Yanshan Street, Yanshan, Guilin 541006, China.
E-mail address: lxr811@glut.edu.cn (X. Luo).

https://doi.org/10.1016/j.apgeochem.2018.07.010
Received 3 May 2018; Received in revised form 10 July 2018; Accepted 12 July 2018
Available online 04 September 2018
0883-2927/

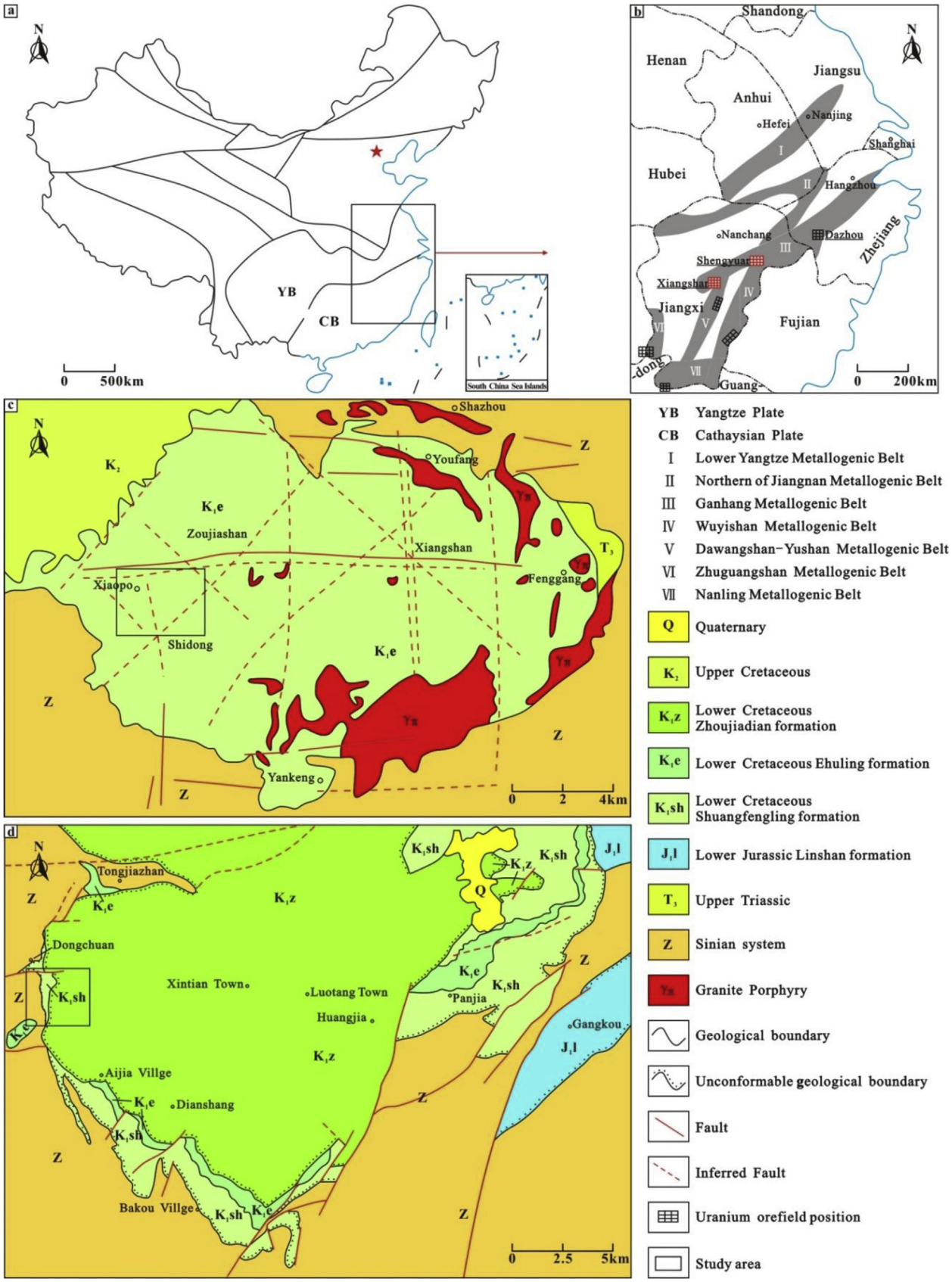

Fig. 1. Location and geological sketch of the study area (a) Location diagram of tectonics; (b) Location diagram of metallogenic belt and uranium field in south-eastern China (Zhong et al., 2015); (c) Geological diagram of Xiangshan volcanic basin (Yu, 2016); (d) Geological diagram of Shengyuan basin (Wu et al., 2002; Liu, 2013).

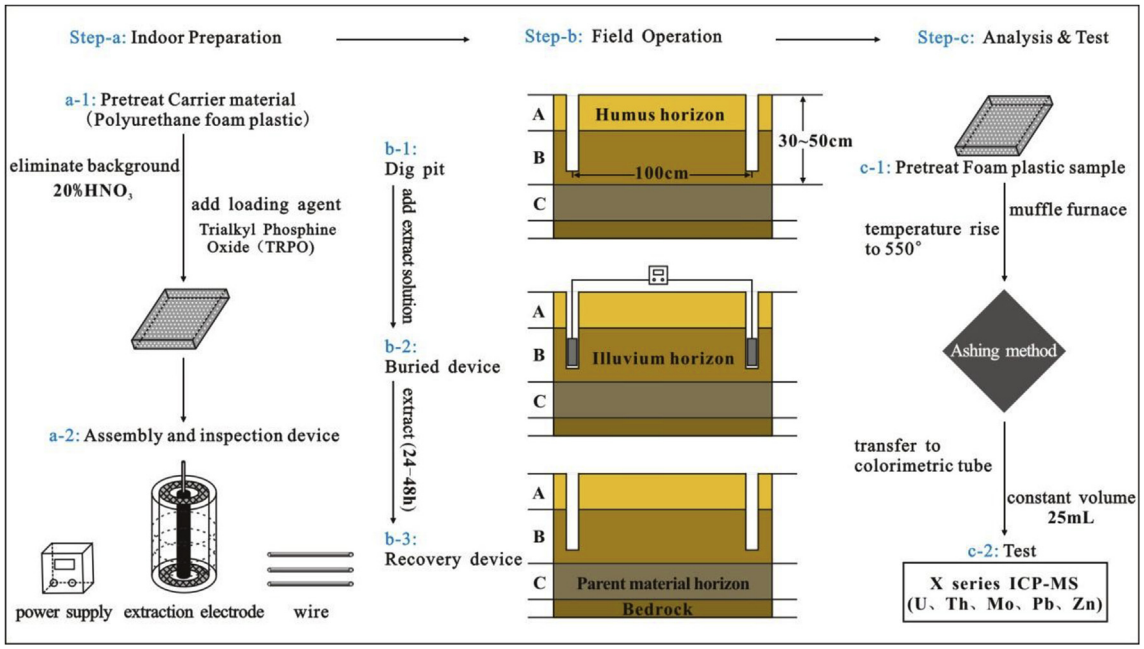

Fig. 2. Workflow chart of the geoelectrochemical probe method.

Table 1
The original data and *CV* of geoelectrochemical measurements of transect#64 in the Julongan deposit from the Xiangshan uranium deposit. Unit of element concentrations is mg/kg; the single-point contrast value may be represented by the equation $CV = C_i/C_0$, in which *CV* is the single-point contrast value, C_i is the content of a certain element and C_0 is the background value of a certain element.

Number	U	*CV*	Th	*CV*	Mo	*CV*	Pb	*CV*	Zn	*CV*	Ag	*CV*
64–1	0.32	1.6	0.05	0.7	0.07	0.6	0.54	14.6	0.27	1.1	0.02	0.7
64–2	0.12	0.6	0.04	0.6	0.09	0.8	0.66	17.8	0.19	0.8	0.036	1.3
64–3	1.32	6.6	0.13	1.9	0.13	1.2	0.87	23.5	0.93	3.9	0.03	1.1
64–4	1.06	5.3	0.11	1.6	0.12	1.1	0.55	14.9	0.29	1.2	0.025	0.9
64–5	0.18	0.9	0.08	1.2	0.12	1.1	0.29	7.8	0.27	1.1	0.026	1.0
64–6	0.17	0.9	0.02	0.3	0.12	1.1	0.33	8.9	0.25	1.0	0.021	0.8
64–7	0.23	1.2	0.03	0.4	0.06	0.5	0.35	9.5	0.22	0.9	0.023	0.9
64–8	0.14	0.7	0.05	0.7	0.06	0.5	0.24	6.5	0.29	1.2	0.023	0.9
64–9	0.63	3.2	0.32	4.8	0.24	2.1	0.92	24.9	1.11	4.6	0.046	1.7
64–10	0.22	1.1	0.07	1.0	0.08	0.7	0.3	8.1	0.27	1.1	0.015	0.6
64–11	0.15	0.8	0.08	1.2	0.11	1.0	0.27	7.3	0.17	0.7	0.028	1.0
64–12	0.11	0.6	0.03	0.4	0.09	0.8	0.23	6.2	0.2	0.8	0.111	4.1
64–13	0.27	1.4	0.11	1.6	0.13	1.2	0.47	12.7	0.85	3.5	0.017	0.6
64–14	0.56	2.8	0.18	2.7	0.18	1.6	0.62	16.8	0.68	2.8	0.034	1.3
64–15	0.24	1.2	0.08	1.2	0.12	1.1	0.36	9.7	0.49	2.0	0.032	1.2
64–16	0.37	1.9	0.04	0.6	0.05	0.4	0.4	10.8	0.23	1.0	0.034	1.3
64–17	0.94	4.7	0.22	3.3	0.25	2.2	1.83	49.5	1.89	7.9	0.083	3.1
64–18	1.23	6.2	0.14	2.1	0.14	1.2	0.75	20.3	0.59	2.5	0.035	1.3
64–19	0.23	1.2	0.07	1.0	0.1	0.9	0.31	8.4	0.24	1.0	0.02	0.7
64–20	0.25	1.3	0.04	0.6	0.17	1.5	0.35	9.5	3.08	12.8	0.029	1.1
64–21	0.28	1.4	0.06	0.9	0.12	1.1	0.39	10.5	2.1	8.8	0.02	0.7
64–22	0.27	1.4	0.1	1.5	0.13	1.2	0.45	12.2	0.32	1.3	0.029	1.1
64–23	0.16	0.8	0.03	0.4	0.08	0.7	0.44	11.9	0.42	1.8	0.035	1.3
64–24	0.13	0.7	0.06	0.9	0.14	1.2	0.22	5.9	0.16	0.7	0.018	0.7
64–25	0.2	1.0	0.06	0.9	0.13	1.2	0.46	12.4	0.56	2.3	0.026	1.0
64–26	0.15	0.8	0.06	0.9	0.13	1.2	0.49	13.2	1.87	7.8	0.046	1.7

surface with an apparatus powered by high power (Ryss and Goldberg, 1973). The method is classified as one of the deep-penetrating geochemical prospecting methods used by mineral explorers around the world since the millennium (e.g., (Xie, 1998; Xie and Wang, 2003). The method has since progressed greatly in terms of methodology and technologies used (Levitski et al., 1996; Leinz et al., 1998; Luo et al., 2002a; Kang and Guo, 2008). Tests and field applications have so far confirmed its efficacy in predicting and locating concealed metal deposits (Smith et al., 1993; Luo et al., 2002b; Luo and Zhou, 2004). The basic operating principle of the method is based on the ion homeostasis in near-surface rocks along with unconsolidated soil and sediment formations. Buried ore bodies are composed of different minerals with different self-potential (metal electrode potential). These bodies may release metal cations through an electrochemical field and form ion halo anomalies on the surface (Luo et al., 2007; Liu et al., 2018). However, the mechanisms behind the element migration from deep within the earth to the surface are not yet well understood. This may partially contribute to the fact that the mechanisms behind observable geoelectrochemical anomalies of these elements are one of the hottest topics and debates in the geochemical prospecting community (Wang, 2005; Kang and Guo, 2008; Sun et al., 2015). Most Chinese researchers believe that the anomalies are the result of a process starting from the

Table 2
Original concentration data and *CV* of geoelectrochemical measurements of transect I-I′ in the 70-deposit from the Shengyuan uranium deposit. Unit of element concentrations is mg/kg, *CV* denotes the single-point contrast value.

Number	U	*CV*	Mo	*CV*	Number	U	*CV*	Mo	*CV*	Number	U	*CV*	Mo	*CV*
I-1	0.08	0.8	0.17	1.1	I-11	0.18	1.8	0.17	1.1	I-21	0.15	1.5	0.35	2.3
I-2	0.02	0.2	0.13	0.8	I-12	0.32	3.2	0.38	2.5	I-22	0.17	1.7	0.21	1.4
I-3	0.03	0.3	0.15	1.0	I-13	0.06	0.6	0.07	0.5	I-23	0.15	1.5	0.18	1.2
I-4	0.02	0.2	0.02	0.1	I-14	0.04	0.4	0.04	0.3	I-24	0.14	1.4	0.15	1.0
I-5	0.05	0.5	0.06	0.4	I-15	0.25	2.5	0.17	1.1	I-25	0.1	1	0.3	2.0
I-6	0.09	0.9	0.09	0.6	I-16	0.08	0.8	0.01	0.1	I-26	0.17	1.7	0.75	4.9
I-7	0.05	0.5	0.24	1.6	I-17	0.5	5	0.49	3.2	I-27	0.14	1.4	1.14	7.5
I-8	0.13	1.3	0.16	1.0	I-18	0.05	0.5	0.03	0.2	I-28	0.07	0.7	0.47	3.1
I-9	0.28	2.8	0.15	1.0	I-19	0.03	0.3	0.06	0.4	I-29	0.03	0.3	0.23	1.5
I-10	0.17	1.7	0.22	1.4	I-20	0.05	0.5	0.21	1.4					

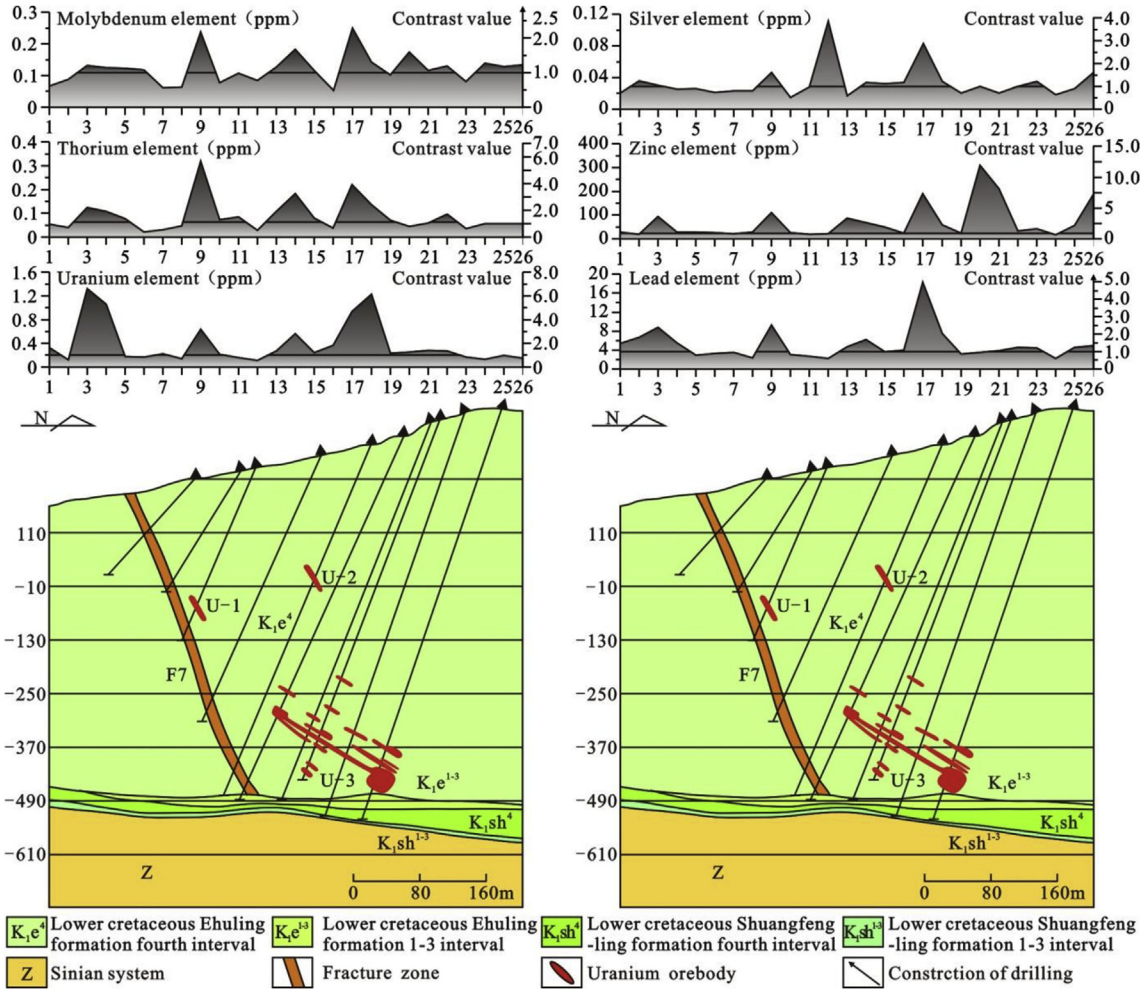

Fig. 3. Geological and geoelectrochemical anomaly profile of transect #64 in the Julongan deposit from the Xiangshan uranium deposit.

electrochemical dissolution of deep ore bodies and ending with certain elements and ions from the bodies migrating up to the sub-surface. This phenomenon is influenced by multiple factors such as circulating deep groundwater, ion diffusion, redox potential and other geochemical gradients, evaporation, and (least accounted for) geogenic gas migration (Luo and Zhou, 2004; Wang, 2005). This paper aims to test the geoelectrochemical method in two well-known volcanogenic uranium deposits (the Xiangshan and Shengyuan deposits in southeastern China) to discuss (i) the mechanisms behind geoelectrochemical anomaly formation, and in particular (ii) to improve the understanding of the element migration from deep ore bodies to the surface that is most likely responsible for the anomaly formation measured by geoelectrochemical devices. Also provided in the paper are some ore prediction studies in the depths of the deposits and peripheral areas as an indicator of further application of this method in China.

2. Geological setting and methods

2.1. Geological setting

The study area is located within the Ganhang metallogenic belt, a transition zone from the Yangtze platform to the South China fold system (Fig. 1a). The Ganhang metallogenic belt contains some of China's largest volcanic rock-hosted uranium deposits, including the

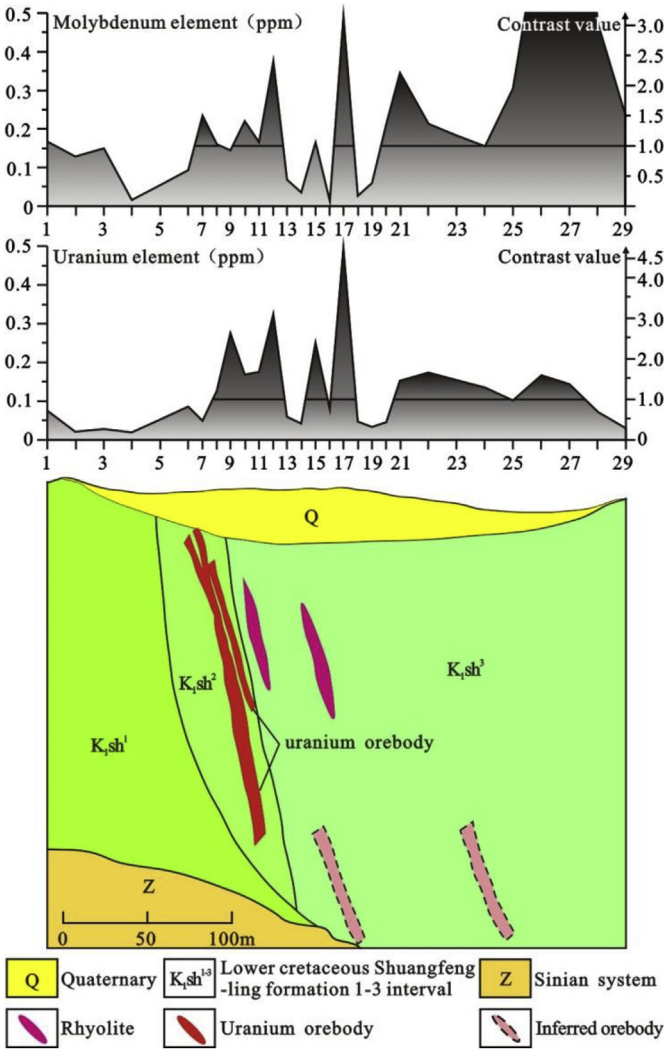

Fig. 4. Geological and geoelectrochemical anomaly profile of transect I–I′ in the #70 uranium deposit from the Shengyuan area.

Dazhou, Shengyuan, and Xiangshan uranium deposits (Fig. 1b). Volcanic rock-hosted uranium deposits in the Ganhang metallogenic belt are mainly buried in collapsed and graben volcanic basins within an activated platform, surrounded by Mesozoic and Cenozoic red graben basins or coal-bearing graben sedimentary basins.

The Xiangshan uranium deposit is entrapped in a volcanic basin of the same name between the Dawangshan-Yushan granite-type uranium metallogenic belt and the Ganhang volcanogenic uranium metallogenic belt, in the south flank of the transit zone or joint zone between the Yangtze platform and South China fold system (Fig. 1b). The basin forms an oval shape with an east-west trending long axis and an exposed collapse caldera of 400 km^2 (Fig. 1c). A Lower Cretaceous Ehuling Formation of purple tufaceous siltstone, fine-grained sandstone and grey tuff rock dominates the main part of the basin. Sinian metamorphic rocks (green schist facies phyllite, slate and metasandstone) with local Triassic coal-bearing systems form the base of the basin (Fan et al., 2005; Zhang, 2005).

The Shengyuan uranium deposit is buried in a subsidence basin of the same name with an outcrop area of 416 km^2 (Fig. 1d). Volcanic rocks in the Shuangfengling and Ehuling Formations of the Wuyi group form an unconformable contact with underlying Sinian metamorphic rocks at the margin of the basin and lower Jurassic coal-bearing clastic rocks in the northeast part of the basin. A series of massive red clastic rocks of the upper Zhoujiadian Formation in the lower Jurassic covers the central area of the basin (Wu et al., 2002).

Previous studies showed that the volcanogenic uranium deposits are closely related to a process starting with differentiated uranium-bearing volcanic gas or liquid flowing upward along early-formed volcanic feeders. Upon reaching some tectonic weak spots (convergence sections of EW- with NE-NNE- or NW-oriented tectonic structures in the study area, for example), the ore minerals were precipitated by means of vein filling or replacement caused by a sudden temperature and pressure dropdown and a pH change from acidic to weakly alkaline. The uranium was dissolved in the ore-forming solution in the form of uranyl carbonate complexes, ($[UO_2(CO_3)_3]^{-4}$, $[UO_2(CO_3)_2]^{-2}$), and a fluoride complex, $[UO_2F_3]^-$, which are highly soluble in hydrothermal solutions (Yang and Wang, 1999). Upon reacting with surrounding rocks, the $UO2^{2+}$ was reduced to form mostly pitchblende along with some coffinites with scattered Th-pitchblende and brannerite mineralizations. Uranium ore bodies are generally associated with enrichments of other trace metals, such as Mo, Th, F, Fe, Be, Au, and Zn/Pb, among which Mo, Th, and Be can be comprehensively utilized together with the uranium.

2.2. Materials and methods

Two representative transections were selected, which included transect #64 in the Julongan ore body from the Xiangshan uranium deposit and transect I-I′ in the #70 ore body from the Shengyuan uranium deposit in Jiangxi Province. With a 20-m spacing (locally 10-m spacing) sampling layout, a total of 55 sampling points were arranged in both areas.

Fig. 2 presents a scheme of the geoelectrochemical method workflow, which has been detailed previously (Liu et al., 2015, 2017). The geoelectrochemical extractor probes are composed of high-density polyether urethane foam with TRPO (trialkyl-phosphine-oxide) as the loading reagent, together with wire, filter paper, and carbon rods. The probes are placed into the soil down to the B-horizons less affected by humus and organic litter to electrochemically scavenge the trace elements from soil pore water over 24 h, with the extraction fluid in the foam as an activator. Subsequently, the foams are ashed and acid-digested. The final extractant solutions are subsequently analysed for their trace element contents with a US Thermo Elemental X series inductively coupled plasma mass spectrometer (ICP-MS) in the analytical centre of China Nonferrous Metals (Guilin) Geology and Mining Co. Ltd. The analytical quality assessment is the same as that which was earlier reported in detail (Shi et al., 2009).

Element concentration data for all the electrochemical probe extractant samples are listed in Tables 1 and 2. To eliminate the interference between the measurement scale, dimension, and elemental background values, the “single-point contrast value method” is used in the production of the anomaly map. The single-point contrast value (*CV*, dimensionless) refers to the ratio of original value to background solute value of a certain element at each sampling point. With a $CV > 1$, we may presume relative enrichment of elements, and with a $CV < 1$, we may infer relative depletion of elements (Zhang et al., 2015). The *CV* factors are therefore used to indicate the enrichment or depletion of certain elements by the geoelectrochemical probe material. The foams were also analysed for scavenged nanoparticles using a scanning electron microscope equipped with an X-ray energy-dispersive analyser as detailed previously by Wang et al. (2017).

3. Results and discussion

3.1. Geoelectrochemical anomalies for the volcanogenic uranium deposits

3.1.1. Geoelectrochemical anomalies of transect #64

The ore bodies shown as multibranched shapes in the transect #64 are buried at depths of between 250 m and 470 m, in a 0–10° direction with a dip angle of 60–65° (Fig. 3). They occur mainly in mortar lava as

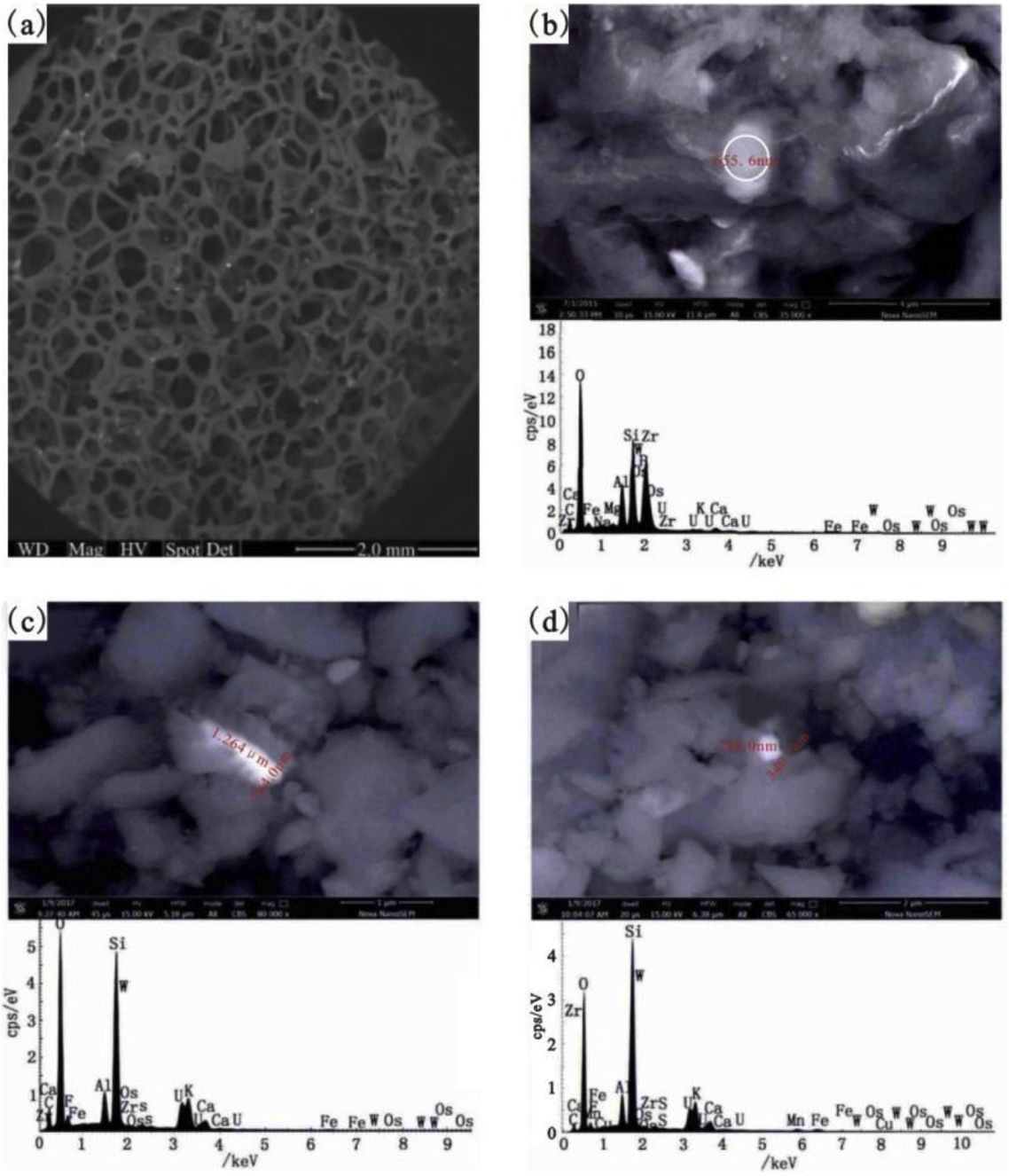

Fig. 5. Mineralization-related nanoparticles photos for (a) absorption of nanoparticles scavenged in the geoelectrochemical extraction foam exposed in the surface soil above the uranium ore body (Sun et al., 2015); (b)–(d) the nanoparticles containing U (Wang et al., 2017).

veins, lenses or cryptomeres, with U grades varying from 0.14% to 0.4%. Geoelectrical anomalies of the elements U, Th, and Mo were observed most frequently between measuring points No. 8 to No. 20 above known ore bodies. The width of the anomaly data spread corresponds well with the range of the ore bodies. A maximum electrochemically derived U extractant concentration anomaly value of 1.23 ppm (averaged at 0.46 ppm) was measured at sampling point No. 18 with an average *CV* of 2.4. The mean Th concentration anomaly value was 0.14 ppm with the maximum value measured at sampling point No. 9 with an average contrast of 2.1. Mo concentration anomalies were averaged at 0.18 ppm with the maximum value of 0.25 ppm at sampling point No. 17 with an average contrast of 1.6. Zn concentration anomalies were distributed largely between sampling points No. 16 to No. 22 matching well with the location of a deep ore bodies U-3, while Pb and Ag anomalies found between sampling points No. 8 and No. 10, as well as No. 16 and No. 19, were mainly distributed above shallower ore bodies (U-1 and U-2). The Zn anomaly values averaged at 160 ppm with the maximum value of 308 against an average contrast of 6.7. Pb anomalies peaked at point No.17 and averaged at 0.39 ppm with an average contrast of 10.6. Ag anomalies were averaged at 0.062 ppm with a maximum at 0.11 ppm found at point No. 12 with an average contrast of 2.3. The evident U and Pb anomalies between points No. 2 to No. 5 were thought to be caused by a secondary effect due to the F7 fracture zone.

3.1.2. Geoelectrochemical anomalies of transect I-I′

Ore bodies shown in transect I-I′ were found to be lamellar or quasi-lamellar (Fig. 4) and 100–378 m in length (maximum length of 490 m)

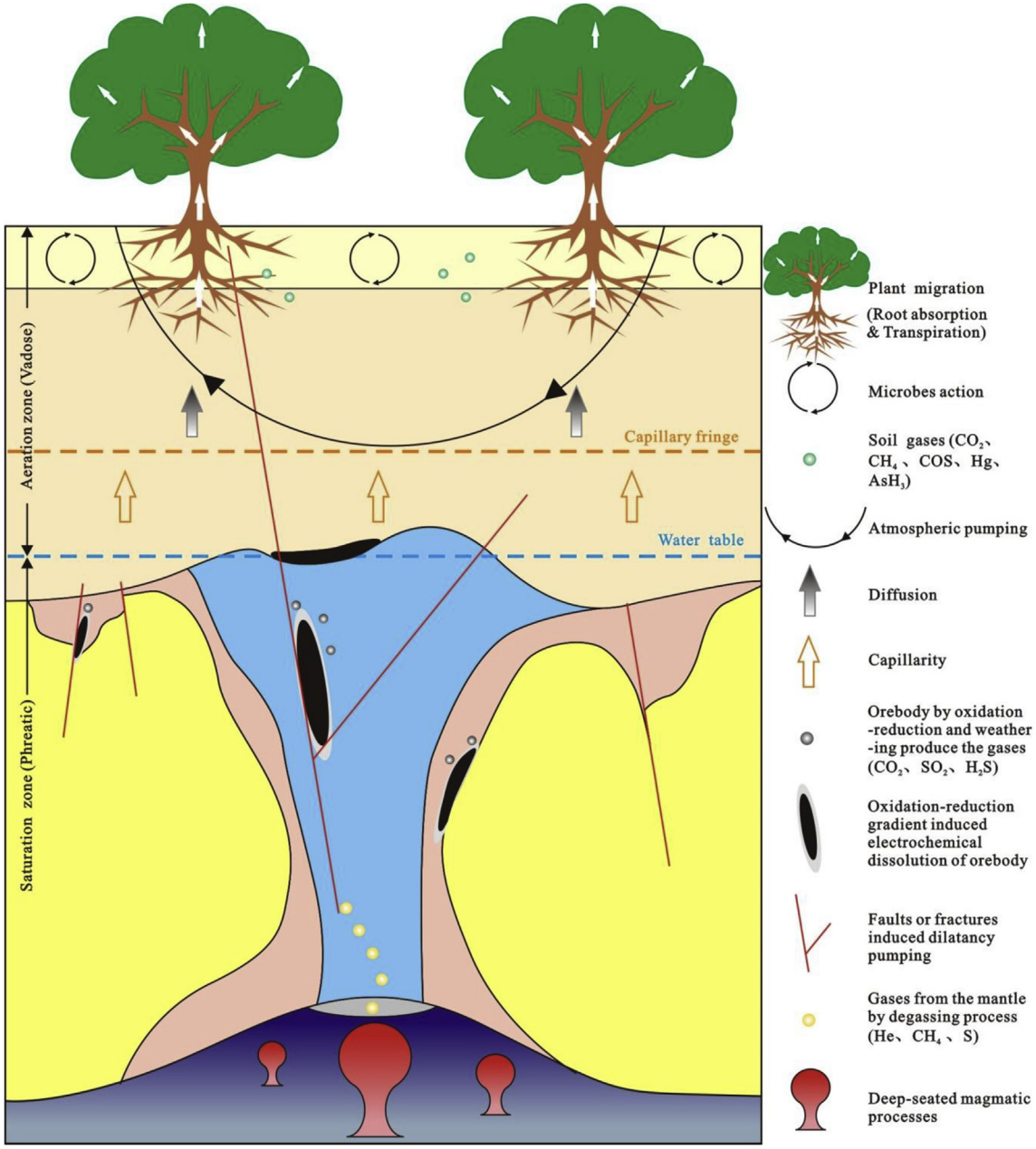

Fig. 6. Migration model of mineralization-related nanoparticle migration of volcanic-type uranium deposit.

and 4 m in thickness, with U grades of 0.06%–0.2% (peaking at 3%) in bed-parallel fracture zone of ignimbrites. Uranium concentration anomalies were found between sampling points No. 8 and No. 13 with an average value of 0.21 ppm against an average contrast of 2.1. They correspond to the location of known ore bodies. The anomalies had an averaged value of 0.37 ppm between points No. 14 to No. 17, and an averaged value of 0.16 ppm against an average contrast of 1.5 between points No. 20 to No. 28. All these measurements indicated that there were buried uranium deposits deep under the anomalies.

Molybdenum concentration anomalies were found between points No. 6 to No. 13 with an average value of 0.23 ppm against an average contrast of 1.5, matching perfectly with the locations of known ore bodies. No. 17 represented a singular anomaly point with a value of 0.49 ppm. Measurement of samples from points No. 20 to No. 29 showed an averaged value of 0.43 ppm against an average contrast of 2.7. The Mo anomalies also indicated the potential for deeply buried uranium deposits. Analyses of the above anomalies in the typical sections of the two lines show that obvious anomalies of U and Mo above blind structures and ore bodies are captured with an average contrast ranging between 2.1 to 2.3 and 1.5 to 1.6, respectively. If Th, Pb, Zn, and Ag anomalies also accompany the U anomalies, the potential for discovering deeply buried ore deposits is greater.

3.2. Detection of mineralization-related particles

Some nanoscale U-bearing mineral particles in geoelectrochemical probe foams were found under the scanning electron microscope (Fig. 5). The size of uranium particles in the soil is 600–700 nm, and they are adsorbed on the surface of clay minerals in a single or polymerized form, which is similar to those of uranium particles in deep ores in terms of component characteristics. This may suggest that nanoscale uranium mineral particles moved up from the ore body to the near-surface. The migration process thus not only enriches mineralization-related elements in the soil pore water but also drives

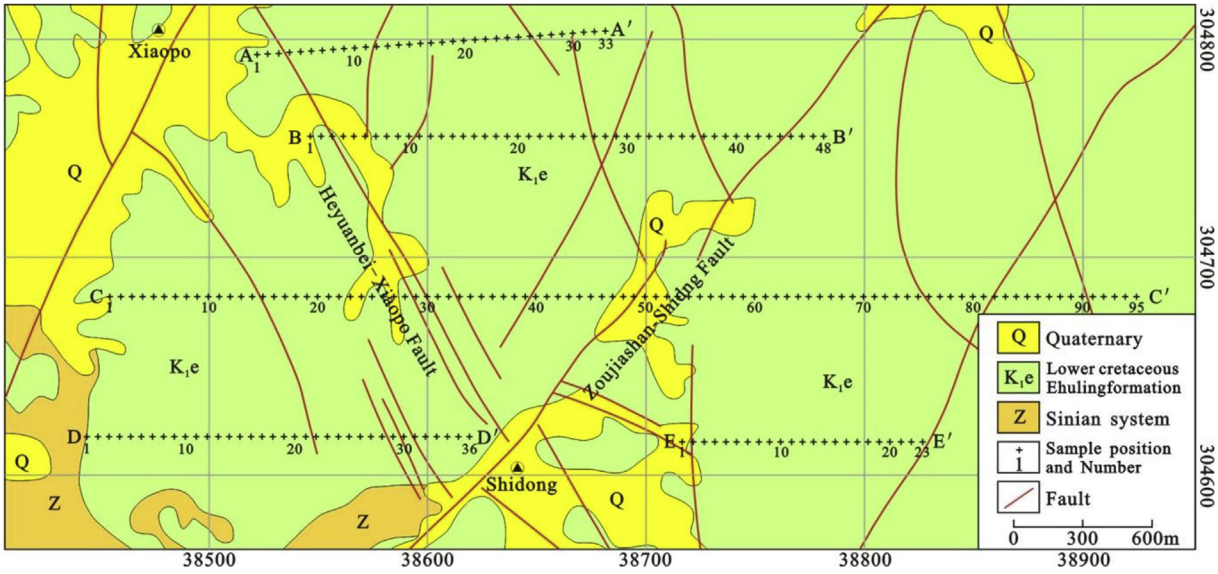

Fig. 7. Geological and work deployment diagram of the Shidong area.

Table 3
Statistics of geoelectrochemical content data parameters in the Shidong area. The element obeys a logarithmic normal distribution after high or low values are eliminated, the background value is the geometric average value of the element, and the calculation formula is $C_0 = \sqrt[n]{c_1\ c_2\ c_3.....c_i}$, in which C_0 is the background value, c_i is the content of a certain element and n is the total number of samples.

Element	U	Th	Mo	Cu	Pb	Zn
Number	199	172	194	174	211	212
Maximum	4.42	5.59	8.21	224.6	51.08	54.9
Minimum	0.068	0.032	0.14	1.1	2.03	1.45
Average	0.54	0.36	0.65	12.08	6.48	9.07
Standard deviation	0.68	0.52	0.69	30.4	5.21	7.16
Variation coefficient	1.27	1.43	1.06	2.52	0.8	0.79
Background value	0.34	0.17	0.45	3.12	5.24	7.36

nanoparticles to move though at least a limited distance and range. Ore bodies in volcanogenic uranium deposits are typically a mixture of uraninite, coffinite, brannerite, and uranothorite, with a variety of accessory metallic ore minerals such as molybdenite, pyrite, galena, and sphalerite, as well as uranium-bearing minerals such as zircon and apatite. These deeply buried ore bodies are seldom weathered directly by the anoxic formation water.

For the upward migration of mineralization-related colloids and nanoparticles scavenged by the geoelectrochemical probe foams, two factors are theorized to be mostly responsible, including (i) the aqueous medium as solute carrier and (ii) the upward driving forces provided by concentration, temperature, and pressure gradients as well as geogenic gas advection (Fig. 5). Vertically moving geogenic gases are mostly driven by temperature and pressure gradients, and may take some mineralization-related nanoparticles with them when they pass by ore bodies or ore-bearing rocks (Klusman, 1993). Swedish researchers confirmed the existence of ascending geogas flux through measurements of Rn above some buried uranium deposits (Kristiansson and Malmqvist, 1982; Malmqvist and Kristiansson, 1984). Geogenic gas advection is related mostly to CO_2, He, and CH_4 vented from mantle sources (Gold and Soter, 1980). Biomethylation of metalloids such as As, Se, Mo, Bi and Sb might accelerate the migration of the ore-indicating nanoparticles as well (Klusman, 1993; Hirner et al., 1998). Moreover, biogenic gases released through biological processes from within critical aeration zones may contribute as well (Wang, 2005). In any case, nano-particle migration is accelerated through rapid advective gas flux rather than diffusive solute concentration gradients alone in the deep saturated orebody zone.

Nano- or sub-micrometre-scale particles were identified in ore bodies buried deep during surveys for gold and polymetallic ores. It was suggested that these particles, by means of geogas flux, electrochemical gradients, concentration diffusion, and other methods, move upward to the surface and form weak anomalies (Wang and Ye, 2011; Ye et al., 2014). Recent studies showed that buried hydrothermal uranium deposits in the Hongshanzi basin of Inner Mongolia contain U-bearing nanoparticles at a submicron scale (250–350 nm). Topsoil above these deposits was also found to contain U-bearing particles of a sub-micrometre scale with similar compositions occurring in surface particles in clay or feldspar (Wang et al., 2017). A summary scheme for mineralization-related nanoparticle migration from volcanogenic uranium deposits is depicted in Fig. 6.

3.3. Application in ore prospecting

The Shidong area in the Xiangshan uranium deposit was chosen to test how well the model works in actual ore prospecting. Fig. 7 illustrates the geological map of the block and the measurement points to be followed. The lower Cretaceous Ehuling Formation is dominated by mortar lava and rhyodacite outcroppings in the block. In the southwestern part of the block, the Sinian metamorphic rocks of slates, phyllites, schists, and metamorphic sandstones form the base of the basin on which the block sits. Overlaying Quaternary layers can be discerned from place to place in the central and eastern parts. Faults and fractures are fully developed in the block with a fracture zone of an inverted triangle composed of a NE-trending fault (Zoujia-Shidong fault) and a NW-trending fault (Heyuanbei-Xiaopo fault) as the controlling structures. Secondary NW fracture zones were observed to be developed at the flanks of the triangle. About five survey transects with 235 measuring points were laid out northeastward across the block. Sampling was carried out precisely according to the standard geoelectrochemical procedure (Fig. 2). Anomalies were mapped with a “single point anomaly *CV*” method.

3.3.1. Geoelectrochemical parameter statistics

Statistical data of the elements can be used to some extent to predict ore bodies. Table 3 lists geoelectrochemical parameters of the block. It is obvious that the gap between the minimum and maximum values is quite large: a 50-fold difference for elements U, Th, and Mo, and a 25-

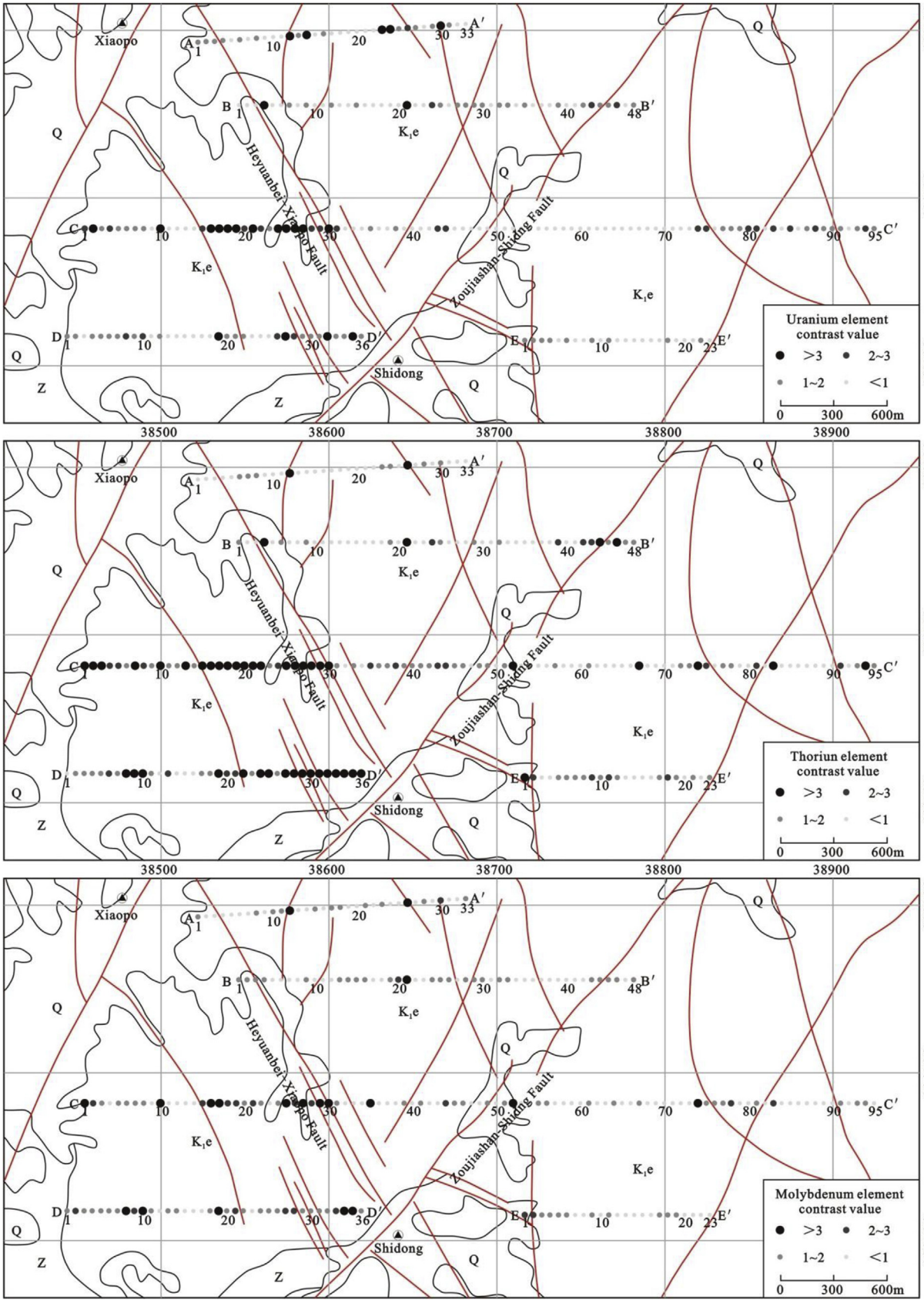

Fig. 8. Distribution map of geoelectrochemical U, Th and Mo element contrast values (*CV*) for the Shidong area.

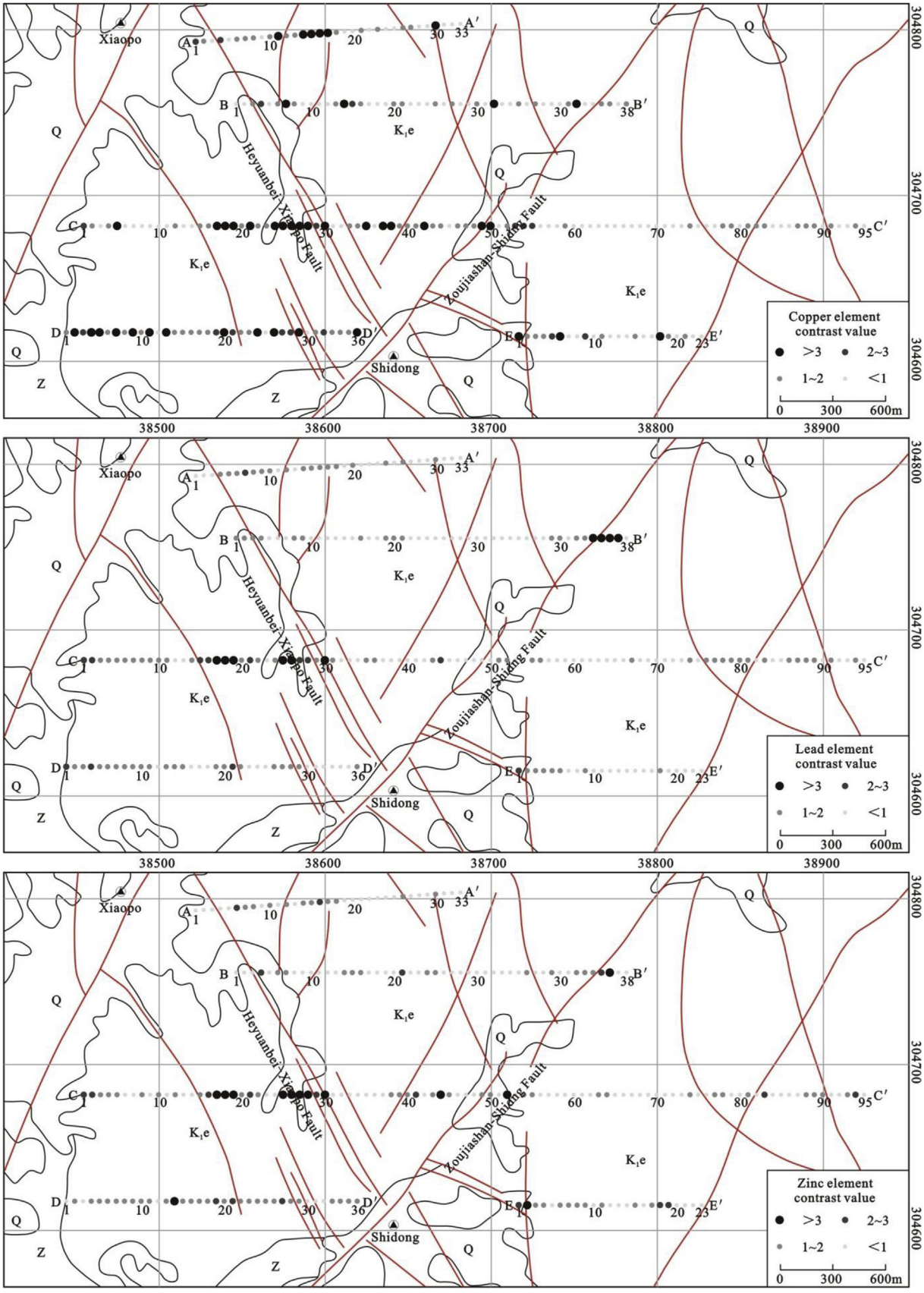

Fig. 9. Distribution map of geoelectrochemical Cu, Pb and Zn element contrast values (*CV*) for the Shidong area.

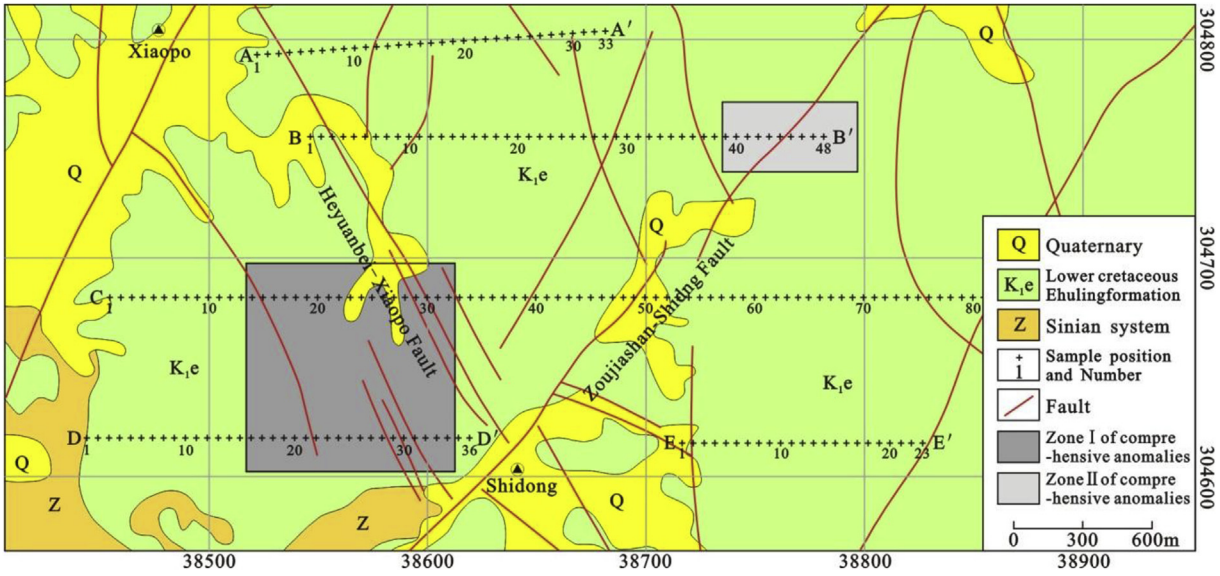

Fig. 10. Comprehensive anomaly planar figure of geoelectrochemical probe of the Shidong area.

fold difference for elements Cu, Pb, and Zn. For Cu, the 204-fold difference between its minimum and maximum values is even larger. Such a considerable deviation may suggest a high degree of dispersion of the elements in the block. The differentiation of the elements can be determined with variable coefficients (ratios of standard deviation over mean standard deviation). By comparing the coefficients of the elements (Zn(0.79) < Pb(0.80) < Mo(1.06) < U(1.27) < Th(1.43) < Cu (2.52)), highly differentiated elements such as U, Th, Mo, and Cu, which have coefficients large than 1, can be distinguished from the moderately differentiated elements Pb and Zn, having coefficients ranging between 0.5 and 1. The background values of these elements (important indicators of geochemical anomalies in a survey) are all lower than the average element content, because there are extreme high and low content values that need to be removed during the calculation of the background value.

3.3.2. Planar distribution of anomalies

Fig. 8 and Fig. 9 shows the distribution of geoelectrochemical contrast anomalies of elements U, Th, Mo, Cu, Pb, and Zn, based on three categories of *CV*: low (1–2), medium (2–3) and high (> 3). The figure reveals first that the three elements U, Th, and Mo with high CV at sampling points No. 15 to No. 31 of transect C, and No. 19 to No. 35 of transect D, were located along the southeast end of the Heyuanbei-Xiaopo fault and near the secondary fracture zone. Sampling points No. 74 to No. 95 of transect C, with mostly medium to low *CV* of Th and Mo, and No. 32 to No. 38 of transect B, are set above mortar lava and rhyodacite of the Ehuling Formation (K_1e). Transects A and E revealed largely low *CV* with some medium to high values at certain locations, corresponding to the whereabouts of the fault. Second, the distribution of *CV* of the elements Cu, Pb, and Zn is consistent with statistical results of geoelectrochemical parameters with Cu having more medium to high *CV*. Medium to high *CV* (of mostly Cu) are generally distributed between sampling sites No. 16 to No. 30 of transect C and No. 19 to No. 32 of transect D. Medium to high *CV* for the elements Pb and Zn are scattered between points No. 16 to No. 31 of transect C, corresponding to the southeast end of the Heyuanbei-Xiaopo faults and a secondary fracture zone. High *CV* for the element Cu was found between points No. 11 to No. 17 of transect A and medium to high *CV* at some singular points of other transects.

3.3.3. Prediction of ore bodies

We encircled two anomaly zones (with their boundary extended outward by a 1/4 line spacing in Fig. 10) based on the geological conditions of the block and the distribution pattern of element *CV*. Analyses of the two zones show that Zone I lay between points No. 14 to No. 32 of transects C and D, with an area of 0.81 km^2 and an average *CV* > 2 (wherein the elements had mostly medium to high *CV* with U at 3.44, Th at 5.77, Mo at 2.56, Cu at 6.92, Pb at 2.00, and Zn at 2.03). Zone I was located near or in the intersection of the Heyuanbei-Xiaopo and Zoujiashan-Shidong faults as well as a secondary fracture zone. Outcropped Ehulin Formation with mortar lava and rhyodacite could already be discerned in the field. The latest study of the area suggested that the distribution of uranium ore bodies in the central and western parts of the Xiangshan deposit was mainly controlled by a NE-trending faulted structure belt, with the Zoujiashan-Shidong fault zone playing the most important role and the intersection of tectonic syntax determining the placement of ore bodies. Medium to high *CV* of U and Th were found to be imposed by values of Cu, Mo, Pb and Zn, indicating great potential for mineralization in the zone.

On the other hand, Zone II was identified in between points No. 29 to No. 38 of transect B, with an area of 0.18 km^2 and average *CV* > 1 (wherein the elements had mostly low *CV* with U at 1.40, Th at 1.80, Mo at 1.16, Cu at 1.37, Pb at 2.05 and Zn at 1.44). It was located on the Zoujiashan-Shidong fault belt along with outcropped mortar lava and rhyodacite of the Ehuling Formation. Analyses show that mortar lava and rhyodacite served as surrounding rocks for Pb-Zn mineralization in the Xiangshan deposit. Judging by the high average *CV* of Pb, Zn, and Th, we believe that the opportunity to find Pb-Zn ore bodies in this zone is promising.

4. Conclusions

(1) Analyses of geoelectrochemical anomalies presented in representative sections from the transect #64 crossing the Julongan ore body in the Xiangshan uranium deposit, and the transect I-I′ through the #70 ore body in the Shengyuan uranium deposit, both show that distinct geoelectrochemical anomalies of U and Mo were captured above deep ore bodies. The average anomaly contrast values ranged from 2.1 to 2.3 and from 1.5 to 1.6, respectively, corresponding perfectly to the locations of known ore bodies. Anomalies of Th, Pb, Zn, and Ag were also tested, confirming the viability and effectiveness of using the geoelectrochemical probe method to locate buried uranium deposits in the study area.
(2) The geoelectrochemical anomaly detection was corroborated by

detection of U-bearing nanoparticles scavenged in the probe foams. Migration models for the particles are proposed in terms of advective forces including geogenic and biogenic gas advection. The nanoparticles could combine with gas bubbles through a flotation-like mechanism, accelerating upward migration directly to the near-surface. When reaching the near-surface, the particles are very likely to be scavenged by all kinds of soil minerals such as clays, oxides, organic colloid substances and more, which are enriched to form various secondary uranium halos or weathered and dispersed to generate pore water solute anomalies.

(3) Prospecting for ore bodies by using the geoelectrochemical anomalies in the Shidong block of the Xiangshan deposit shows positive results. We could differentiate two general geoelectrochemical anomaly zones. Zone I contains anomalies of mostly U and Th (together with Cu, Mo, Pb and Zn) with high *CV* (> 2). Taking into consideration the fact that the zone is located in the NW-trending fault and secondary fault belts and with favourable mineralization conditions, we suggest that the zone should be the target of subsequent exploration efforts. Zone II contains anomalies of low *CV* (> 1) with Pb, Zn, and Th having relative higher values. We suggest the potential for lead and zinc ore deposits deep within this zone.

Acknowledgements

This study is supported by the National Key R&D Program of China (Grant No. 2016YFC0600603 & 2017YFC0602604).

References

Fan, H.H., Wang, D.Z., Shen, W.Z., Liu, C.S., Ling, H.F., 2005. Formation age of the intermediate-basic dikes and volcanic-intrusive complex in Xiangshan, Jiangxi Province. Geol. Rev. 51, 86–91 (in Chinese with English abstract).

Fang, X.H., 2009. Principal geological characteristics of the volcanic type uranium deposits in China. Uranium Geol. 25, 98–104 (in Chinese with English abstract).

Fang, X.H., Fang, M.L., Luo, Y., Liu, R.R., Liu, Q., Zhang, M.L., Wang, S.H., Liu, H., Fu, J., Wang, Y.Z., Zhang, J.W., Xie, Y.C., 2012. The potential evaluation of volcanic type uranium resources in China. Uranium Geol. 28 342-348 + 354 (in Chinese with English abstract).

Gold, T., Soter, S., 1980. The deep-earth-gas hypothesis. Sci. Am. 242, 154–161.

Hirner, A.V., Krupp, E., Schulz, F., Koziol, M., Hofmeister, W., 1998. Organometal(loid) species in geochemical exploration: preliminary qualitative results. J. Geochem. Explor. 64, 133–139.

Hou, D.M., Luo, X.R., Wang, J.L., Wen, M.L., Yang, F.O., Li, Z.Y., 2012. A comparative study of the prospecting for hidden uranium deposits by applying geo-electrochemical method in China and Australia. Geol. Bull. China 31, 126–135 (in Chinese with English abstract).

Jin, H.H., Zhang, H., Liu, Q.D., 2007. Analysis of prospecting effect of polonium survey and geoelectric survey extracted uranium and molybdenum in the south of Shengyuan volcanic basin. Uranium Geol. 23 101-108 + 128 (in Chinese with English abstract).

Kang, M., Guo, L., 2008. The formation of halos. CHIM. Bulletin of Mineralogy, Petrology and Geochemistry 27, 195–199 (in Chinese with English abstract).

Ke, D., Song, L., Wu, G., Wang, Y., 2014. Preliminary studies of CHIM electrogeochemical method at volcanic-type uranium Deposits,Xiangshan basin,China. Acta Geol. Sin. 88, 1362–1363.

Klusman, R.W., 1993. Soil Gas and Related Methods for Natural Resource Exploration. Wiley, New York.

Kristiansson, K., Malmqvist, L., 1982. Evidence for nondiffusive transport of 86Rn in the ground and a new physical model for the transport. Geophysics 47, 1444–1452.

Leinz, R.W., Hoover, D.B., Fey, D.L., Smith, D.B., Patterson, T., 1998. Electrogeochemical sampling with neochim — results of tests over buried gold deposits. J. Geochem. Explor. 61, 57–86.

Levitski, A., Filanovski, B., Bourenko, T., Tannenbaum, E., Bar-Am, G., 1996. "Dipole" CHIM: concept and application. J. Geochem. Explor. 57, 101–114.

Li, S.Z., Luo, X.R., Tang, Z.X., Li, B.H., 2012. Prediction of concealed uranium lead - zinc deposits by geo-electro chemical method in Xiangshan region, Jiangxi province. Miner. Deposits 31, 857–858 (in Chinese with English abstract).

Liu, H.J., Wu, G.D., Xie, S.K., 2017. The preparation method of electrogeochemical extraction adsorption materials for uranium. World Nuclear Geoscience 34, 32–35 (in Chinese with English abstract).

Liu, P.F., Luo, X.R., Wen, M.L., Zhang, J.L., Gao, W., Ouyang, F., Duan, X.C., 2018. Using electrogeochemical approach to explore buried gold deposits in an alpine meadow-covered area. Acta Geochimica 37, 402–413. https://doi.org/10.1007/s11631-017-0258-z.

Liu, P.F., Wen, M.L., Yang, L.K., Li, Y., 2015. Geo-electrochemical extraction technology test and the prospecting prediction in cold plateau area. Chin. Geol. 42, 2000–2007 (in Chinese with English abstract).

Liu, Q., 2013. Chronological and Geochemical Characteristics of Andesites in Shengyuan Uranuim orefield. East China University of Technology, Master.

Luo, X.R., Chen, S.M., Du, J.B., Hu, Y.H., 2002a. Study of geoelectro-chemical method in search for different hidden deposits. J. Mineral. Petrol. 22, 370–372 (in Chinese with English abstract).

Luo, X.R., Kang, M., Ou Yang, F., Wen, M.L., Hou, B.H., 2007. Halo-porming Mechanism, Methodology and Application of Geo-electrochemical Technology in Exploration for mineral Deposits. Geological Publishing House, Beijing.

Luo, X.R., Wang, G.Q., Du, J.B., Hu, Y.H., 2002b. The geo-electrochemical anomaly feature mechanism and finded ore extrapolate for stibium deposit. Geol. Prospect. 38, 59–62 (in Chinese with English abstract).

Luo, X.R., Zhou, T.F., 2004. Feature and forming mechanism of geo-electrochemical anomaly of the Hongqiling copper -nickel deposit and its prediction, Jilin Province. J. Jilin Univ. (Earth Sci. Ed.) 34, 304–308 (in Chinese with English abstract).

Malmqvist, L., Kristiansson, K., 1984. Experimental evidence for an ascending microflow of geogas in the ground. Earth Planet Sci. Lett. 70, 407–416.

Man, R.H., Luo, X.R., Yi, C., 2015. Application of the geo-electrochemical method on prospecting for concealed uranium deposits in the Dongsheng area of the Ordos basin. Bull. China Soc. Mineral Petrol. Geochem. 34, 1007–1013 (in Chinese with English abstract).

Ryss, Y.S., Goldberg, I.S., 1973. The method of partial extraction of metals(CHIM)for exploration of ore deposits. Methods tech. Explor. 84, 5–19.

Shi, H.Y., Yang, Z.P., Huang, J.H., Zhou, Q.M., Xiong, C.X., 2009. Determination of trace elements in electrical absorption prospecting polyform sample by inductively coupled plasma mass spectrometry. Spectrosc. Spectr. Anal. 29, 1687–1690 (in Chinese with English abstract).

Smith, D.B., Hoover, D.B., Sanzolone, R.F., 1993. Preliminary studies of the CHIM electrogeochemical method at the Kokomo mine, Russell Gulch, Colorado. J. Geochem. Explor. 46, 257–278.

Sun, B.B., Zhang, X.J., Liu, Z.Y., Zhou, G.H., Zhang, B.M., Chen, Y.D., 2015. A preliminary study of the formation mechanism of the geoelectric chemistry anomaly. Geophys. Geochem. Explor. 39, 1183–1187 (in Chinese with English abstract).

Wang, X.Q., 2005. Conceptual model of deep penetrating geochemical migration. Geol. Bull. China 24, 892–896 (in Chinese with English abstract).

Wang, X.Q., Ye, R., 2011. Findings of nanoscale metal particles: evidence for deep-penetrating geochemistry. Acta Geosci. Sin. 21, 7–12 (in Chinese with English abstract).

Wang, Y., Ye, R., Liu, X.J., Wu, G.D., Wang, D.S., 2017. Deep-penetrating geochemical microscopic evidence in the hydrothermal uranium deposit exploration. World Nuclear Geoscience 34, 167–173 (in Chinese with English abstract).

Wen, M.L., Luo, X.R., Xiong, J., 2011. Electro-geochemical method in search of concealed uranium deposits in a area of Jiangxi province. Miner. Explor. 2, 404–408 (in Chinese with English abstract).

Wu, J.H., Zhou, W.X., Zhang, B.T., 2002. Stratigraphical sequence and geochronology of the late mesozoic era in Jiangxi Province and Northern Guang dong Province. Geol. Rev. 48, 44–53 (in Chinese with English abstract).

Xie, X.J., 1998. Tactical and strategic deep-penetration geochemical surveys. Earth Sci. Front. 5, 2–14 (in Chinese with English abstract).

Xie, X.J., Wang, X.Q., 2003. Recent developments on deep-penetrating geochemistry. Earth Sci. Front. 10, 225–238 (in Chinese with English abstract).

Yang, J.M., Wang, Q.Y., 1999. Uranium migration form and precipitating mechanism of mineralizing solution in an area volcanic rock type uranium deposits. Journal of Central-South Institute of Technology 13, 55–60 (in Chinese with English abstract).

Yao, W.S., Wang, X.Q., Zhang, B.M., Xu, S.F., Shen, W.J., Du, X.M., 2012. Pilot study of deep-penetrating geo-chemical exploration for sandstone-type uranium deposit, Ordos Basin. Earth Sci. Front. 19, 167–176 (in Chinese with English abstract).

Ye, R., Zhang, B., Wang, Y., 2014. Mechanism of the migration of gold in desert regolith cover over a concealed gold deposit. Geochem. Explor. Environ. Anal. 15, 62–71.

Yu, C.D., 2016. Geochemical Studies on Zoujiashan deposit in Xiangshan Uranium Ore Field. East China University of Technology, Master.

Zhang, W.L., 2005. Reverse magmatic evolution series of the Xiangshan volcanic intrusive complex. Chin. Geol. 32, 24–32 (in Chinese with English abstract).

Zhang, Y.J., Luo, X.R., Duan, H.C., Han, C.Y., Yuan, H.Q., Song, Y.W., Li, Z.F., Gao, Y., 2015. Application of geo-electro chemical prospecting method for concealed gold deposit in Liushaogou district of West Qinling Origen. J. Guilin Univ. Technol. 35, 473–481 (in Chinese with English abstract).

Zhong, F.J., Pang, J.Y., Xia, F., Zhang, Y., Liu, G.Q., Liu, Y., Xing, X.Q., Sun, R., 2015. Construction the minerogenetic prediction geological model for volcanic-type uranium deposits and its application in China. J. East China Inst. Technol. 38, 135–143 (in Chinese with English abstract).